Appl. Phys. B 46, 165–173 (1988)

Applied Physics B Photophysics and Laser Chemistry

Pulsed Laser Desorption near a Jet Orifice: Concentration Profiles of Entrained Perylene Vapor

P. Arrowsmith, M. S. de Vries, H. E. Hunziker, and H. R. Wendt

IBM Research Division, Almaden Research Center, San Jose, CA 95120-6099, USA

Received 16 November 1987/Accepted 1 February 1988

Abstract. We have investigated the entrainment in a jet expansion of material vaporized with a laser pulse from a surface below but closely adjacent to the jet orifice. Jets of He and Ar were used as carriers, and perylene was the test substance. Its distribution in space and time far from the nozzle was measured by laser-induced fluorescence and one-dimensional imaging with an optical multichannel analyzer. The width of the perylene concentration profile was found to be much narrower than the width of the gas expansion, especially in He. This makes it possible to extract a useful portion of the entrained material through a skimmer. Depending on the values of experimental parameters, the center of the profile first appears above, on, or below the jet axis and then moves lower with time. Effects of several parameters on shape and time-dependent position of the profile were investigated. The results can be used to optimize the overlap of the concentration pulse with a skimmer or other probe.

PACS: 35.80.+s, 82.80.Di, 47.45.Nd.

Cooling of polyatomic molecules by seeding them into the free jet expansion of an inert gas has led to enormous advances in their spectroscopy [1]. Sharp and greatly simplified vibronic spectra can thus be obtained for molecules whose spectroscopic details are hidden, and whose absorption strength is dispersed, in a featureless continuum of hot bands at higher temperatures. Among many other applications these cold spectra should be useful for positive and interference-free identification of certain compounds. In order to use this technique for involatile materials of high molecular weight it is necessary to generate a sufficiently high vapor pressure without causing extensive, thermal decomposition. A promising method for doing this is pulsed, laser-induced desorption. It has been shown that many molecules can be vaporized from bulk or desorbed from surfaces by a short laser pulse without decomposition where slow heating leads to pyrolysis and surface reactions [2, 3]. The combination of this method with jet cooling, for the purpose of obtaining laser photoionization mass spectra of biomolecules and other complex organic species, has been demonstrated and successfully used in at least two laboratories [4, 5].

We are interested in determining how sensitive laser desorption with jet cooling can be made for identifying specific, high-molecular-weight organic adsorbates on surfaces. There is one factor in the overall detection efficiency which is virtually impossible to estimate and thus must be determined by experiment: The fraction of adsorbate entrained in the jet which will appear in the detection volume. Since only a small portion of the jet can be sampled, it is obviously important to optimize this fraction which is determined by the spatial and temporal distribution of the injected material in the jet expansion. In order to learn how to achieve this optimization, and to estimate the optimal fraction, we have measured concentration profiles of entrained perylene vapor and explored their dependence on the adjustable parameters of the experiment.

Perylene was chosen as a tracer for several reasons: Its low vapor pressure permits films to be kept in vacuum at room temperature. Its rapid, collisionless

relaxation causes fluorescence to be well separated from the excitation wavelength even under collision-free conditions [6]. In addition, it has a high fluorescence quantum yield which makes it possible to profile low concentrations with good spatial resolution along a probe laser beam with an optical multichannel analyzer. Final temperatures were not determined in this study (see, however, the end of Sect. 3), but the desorption spots were located close to the jet orifice since such an arrangement is expected to achieve as much cooling as possible.

1. Experimental

For ease of reference we will describe the experimental arrangement using the coordinate system shown in the right-hand detail of Fig. 1. It has its origin at the center of the jet orifice; x is the vertical and y the horizontal axis perpendicular to the jet axis, z. The sample was a polycrystalline film of perylene evaporated at room temperature onto a gold-plated, rectangular Cu rod 3 mm wide in the z direction and 50 mm long. Its absorption coefficient at the 248 nm desorption wavelength was measured to be $3.5 \times 10^5\ \mathrm{cm}^{-1}$, which is somewhat higher than a published value of $3.1 \times 10^5\ \mathrm{cm}^{-1}$ [7]. Thick (70 nm) and thin (7 nm) films, as determined by quartz crystal balance and the bulk density, were used. The sample rod could be translated accurately in the x and y directions. Above the jet orifice a UV fused silica rod whose dimensions were $3 \times 3 \times 50$ [mm] could be moved in the same manner. The silica rod was used to test for the effects of expansion into a slot defined by its surface and that of the sample. Translated with the silica rod was a thin stainless steel plate containing three apertures which cut out 1 mm diameter desorption spots from the incident 3.2 mm diameter laser beam. The spot centers were located at $z = 0.7$, 1.7, and 2.7 mm from the orifice of the pulsed valve whose diameter was 0.5 mm [8]. These spots will be referred to as the inner, middle, and outer, respectively.

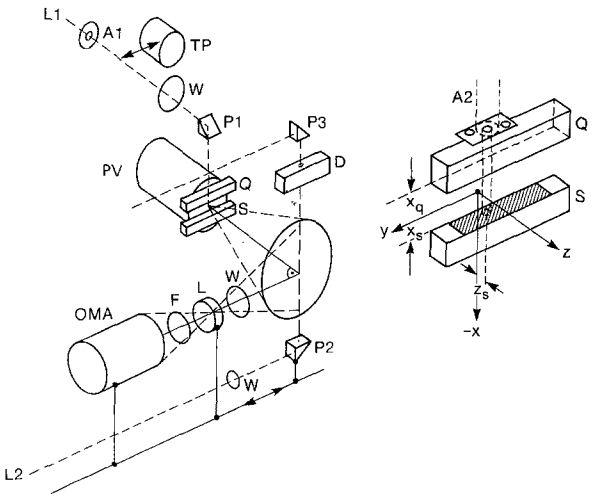

Fig. 1. Diagram of the experimental setup. The detail at right shows the coordinate system and the coordinates for laser desorption. (Abbreviations: A1: 3.2 mm aperture; A2: 1.0 mm apertures (3); D: graphite beam dump with alignment hole; F: Schott GG 400 filter; L: camera lens; L 1: 248 nm excimer laser; L 2: 355 mm Nd/YAG laser; OMA: optical multichannel detector; P 1, P 2, P 3: right-angle prisms; PV: pulse valve; Q: UV fused silica rod; S: sample rod with perylene film; TP: removable thermopile; W: vacuum chamber windows

The sample was vaporized with the unfocused beam of an excimer laser operating at 248 nm (KrF) with 20 ns FWHM pulse duration [9]. Pulse energies measured with a removable thermopile outside the vacuum chamber were varied between 1.5 and 3.2 mJ for the 3.2 mm diameter beam section. Measurements at the sample position with a calibrated pyroelectric film detector [10] showed that this corresponded to 30 to 60 μJ in 1 mm diameter spots at the perylene film.

Concentration profiles of perylene vapor entrained in the jet were measured in an xy plane located at $z = 57$ mm (114 nozzle diameters) from the orifice. At this distance the expansion is collision-free and the profile has reached its final form. A 6 mm diameter probe beam traversed the xy plane in the x direction. The probe was a 6 ns, 20 mJ pulse of 355 nm radiation derived from a Q-switched, tripled Nd:YAG laser [11]. A camera lens (f: 1.8) was used to form an image of the fluorescent probe beam trace on the 3×25 [mm] detector area of an optical multichannel analyzer [12]. Since there were 1024 pixels along the 25 mm detector strip, and the beam trace was demagnified by a 4:1 ratio, the maximum x-resolution (smallest sampling interval) was about 0.1 mm. Most traces were obtained with an x resolution of 0.4 mm, grouping 4 pixels together. The x axis was calibrated by recording the trace of a graduated capillary filled with perylene solution which could be temporarily inserted at the $y = 0$ position. Profiling in the y direction was accomplished with a mechanism which translated a right-angle prism inside the vacuum chamber together with the lens and multichannel detector outside. The width of the probe beam in the y-direction was reduced to 2 mm for these measurements with a horizontal slit placed outside the vacuum chamber window to increase y resolution. Additional details of the experimental arrangement are depicted in Fig. 1.

Pulses derived from a multichannel, computer-controlled delay generator first opened the pulsed valve, then fired the desorption and probe lasers with a variable delay between the latter two. The desorption laser was fired 140 μs after the expansion reached its steady state. No change in concentration profiles was

observed when varying this delay from 0 to 140 μs. Experiments were carried out in single-shot fashion, and 3 (sometimes 10) shots were averaged for each trace. A measurement of the background was obtained in the same manner, except for setting the desorption-probe delay shorter than the perylene arrival time. This background trace was nearly flat and was subtracted from the signal traces. It was due to probe-laser light reflected by the internal surfaces of the apparatus and not completely eliminated by the GG 400 filter. When a series of traces was measured as a function of an experimental parameter the sample was translated in the y direction after each trace, exposing a fresh spot, to minimize effects of sample depletion. Depletion effects were small at the lowest desorption intensity but prominent at the highest one.

The "signal" on the vertical axis in Figs. 2–14 measures total counts for a 0.4 mm sampling interval, accumulated in 3 shots, in units of 10^3, except for Figs. 6 and 8 where it represents counts for a 0.1 mm interval and 10 shots in units of 10^3. The nominal calibration of the detector was 1 count/photon.

2. Results

Since the experimental arrangement is symmetrical about the plane defined by the x and z axes, it is expected that horizontal concentration profiles will reflect this symmetry. The more interesting direction is the vertical (x) where no symmetry is built in. We will first examine profiles in this direction and their dependence on delay time. Experiments described in Sects. 2.1 to 2.4 were carried out with He as the expansion gas, at a source pressure of 1 atm. The effect of the fused silica rod will be described in Sect. 2.4; for all other runs it was positioned at $x_q \geqq 4$ mm where it does not affect the jet expansion. Except for Sect. 2.2 all profiles were measured at the $y=0$ position of the sampling xy plane.

2.1. Vertical Concentration Profiles

Figures 2 to 5 show sequences of vertical concentration profiles recorded as a function of delay between desorption and detection time. As indicated in the captions there is one sequence for each of the four combinations of high and low desorption pulse energy, and short ($z_s=0.7$ mm) and long ($z_s=2.7$ mm) desorption spot distance from the jet orifice. For all of these experiments, the sample was located at $x_s=-0.5$ mm. A 7 nm perylene film was used for the runs of Fig. 3, 70 nm films for all the others.

Examining first the low desorption energy runs in Figs. 2 and 3, it can be seen that the concentration

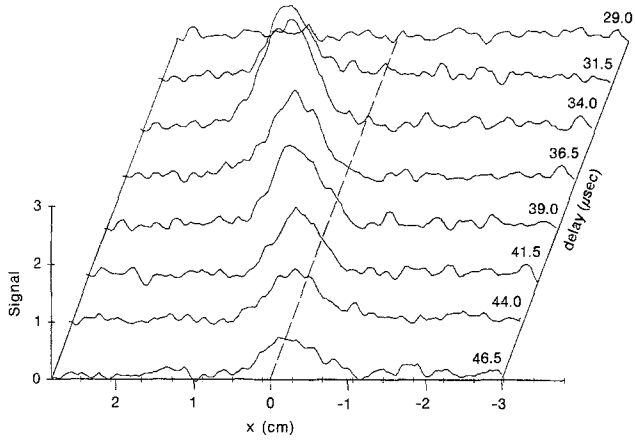

Fig. 2. Time evolution of the vertical concentration profile for the outer spot at low desorption pulse energy. $x_s=-0.5$ mm, $z_s=2.7$ mm

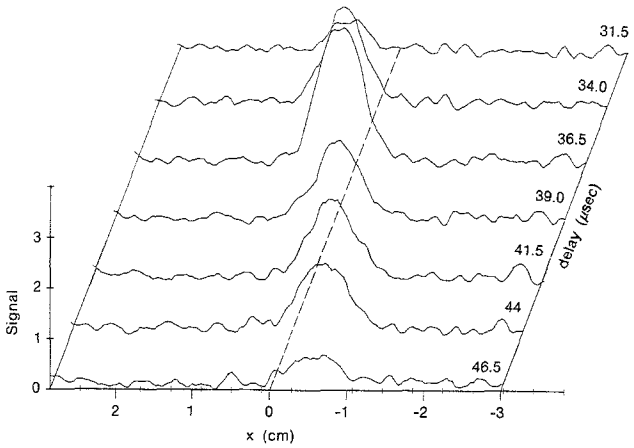

Fig. 3. Time evolution of the vertical concentration profile for the inner spot at low desorption pulse energy. $x_s=-0.5$ mm, $z_s=0.7$ mm

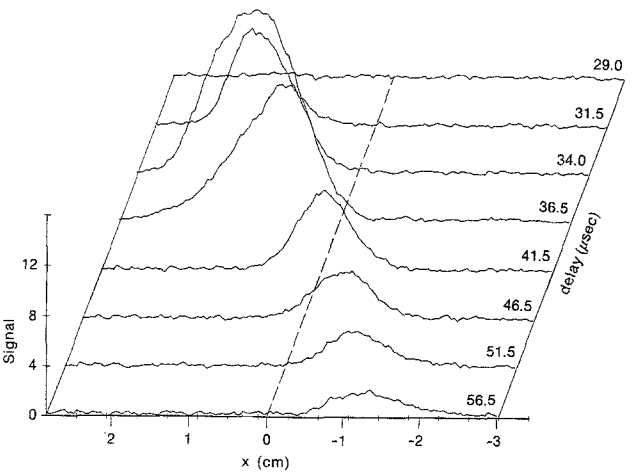

Fig. 4. Time evolution of the vertical concentration profile for the outer spot at high desorption pulse energy. $x_s=-0.5$ mm, $z_s=2.7$ mm

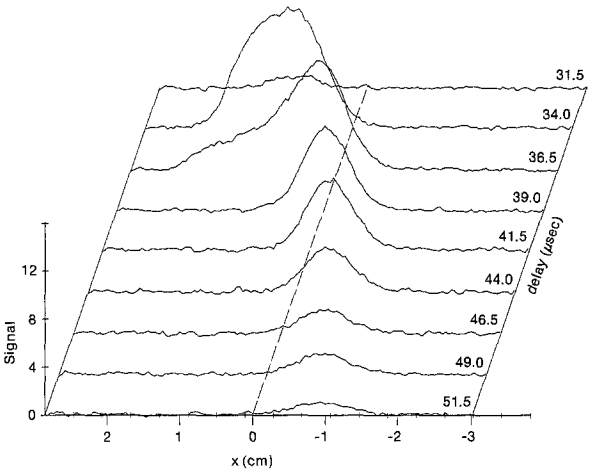

Fig. 5. Time evolution of the vertical concentration profile for the inner spot at high desorption pulse energy. $x_s = -0.5$ mm, $z_s = 0.7$ mm

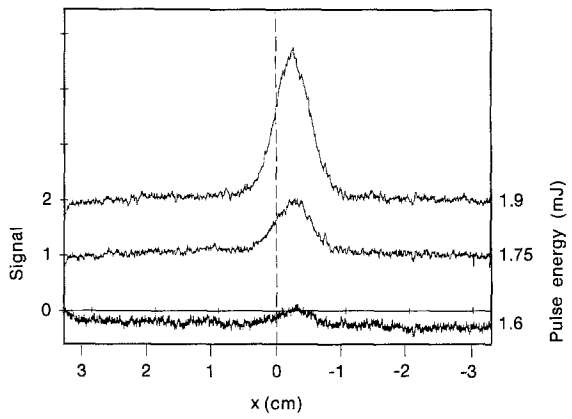

Fig. 6. Effect of desorption pulse energy on signal position and amplitude. $x_s = -0.7$ mm, delay 36.5 μs, 3 mm spot

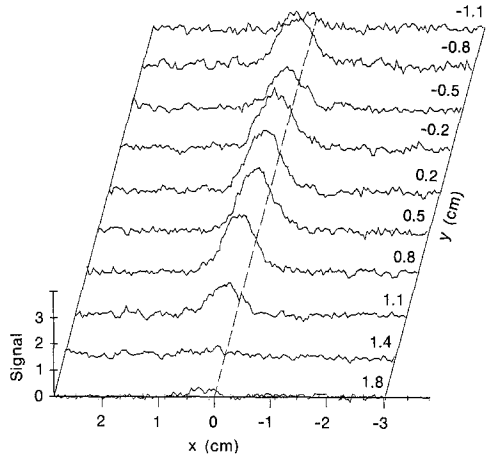

Fig. 7. Two-dimensional concentration profile. $x_s = -0.5$ mm, $z_s = 1.7$ mm, delay 36.5 μs

profiles are quite narrow compared with the FWHM of the density in a free He jet which is 67 mm in the observation plane [13]. The shape of the profile is approximately Gaussian, and its FWHM is about 7 mm independent of delay time. While the early portion of the signal appears well above the beam axis, the center of the profile moves toward and below the axis as the delay is increased. The rate of this motion is about 1 mm/μs. Maximum signal is observed at delays of 36.5 μs for the inner ($z_s = 0.7$ mm) and 34 μs for the outer ($z_s = 2.7$ mm) desorption spot. An undisturbed jet of He has a final velocity of 1.74×10^3 m/s. Thus the perylene flight times for the experimental distances, in a free jet and without velocity slip, are predicted to be 33 and 31 μs. We do not expect exact agreement with experiment since interference of the sample with the jet, as well as the entrainment process, will cause additional delays. The larger distance of the desorption spot from the nozzle decreases the delay of the maximum signal and also has another effect: At equal delay times, the signal maximum from the outer spot lies at higher x values than that of the inner spot.

Before examining the high desorption energy sequences it is useful to remember that the vaporization rate is a very steep (exponential) function of the energy deposited. This is illustrated in Fig. 6 where the energy was varied by inserting fused silica flats in the desorption laser beam. An increase by a factor of 1.2 causes a tenfold increase in signal, from minimum detection level to a size comparable with the maximum signals in Figs. 2 and 3. Note that for these relatively low desorption energies there is no shift in the position of the maximum as the amount of perylene vaporized increases by a factor of 10. This is no longer true at the higher energies used for the runs shown in Figs. 4 and 5.

The most distinct feature in Figs. 4 and 5 is the asymmetrical overshoot of the concentration profile in the positive x direction which occurs approximately at the delay times corresponding to maximum signal in the low energy runs of Figs. 2 and 3. At longer delays this feature disappears and concentration profiles resemble those obtained at low energy. We will discuss this phenomenon in more detail in Sect. 3.1. Maxima at equal delays are located at higher x values for the outer desorption spot, as was the case in the low desorption energy experiments.

2.2. *Two-Dimensional Concentration Profiles*

In order to map the concentration in both x and y directions, a sequence of vertical profiles at different values of y was recorded. Figure 7 shows one such sequence obtained using the middle ($z_s = 1.7$ mm) desorption spot. The shape of the vertical profile remains the same for $y \neq 0$ as it was at $y = 0$. Thus either a graph

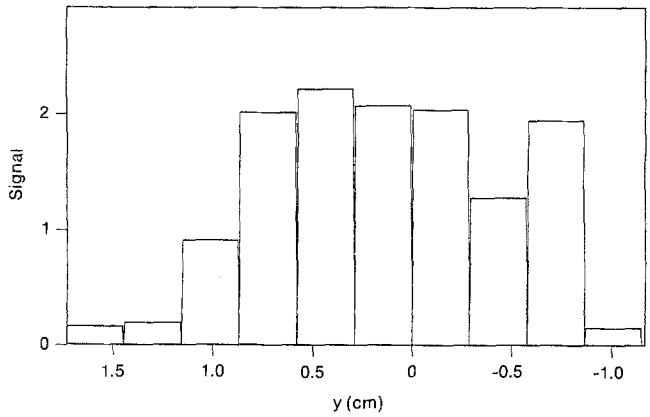

Fig. 8. Horizontal profile obtained by integration along x from the profile shown in Fig. 7

of the maxima in the vertical profiles vs. y or a graph of the total areas under these profiles vs. y will give the same result. The latter method was used to obtain the histogram in Fig. 8. This horizontal profile is somewhat jagged and approximately flat-topped with a FWHM of about 22 mm. It is also roughly symmetrical with respect to $y=0$, as expected.

It proved to be difficult experimentally to obtain smooth horizontal profiles centered on $y=0$. Most of the profiles recorded were actually centered off-axis. Examination of the desorption spots after such experiments revealed that they were themselves shifted from the z axis in the direction in which the center of the profile was located. Thus part of the difficulty originated from the lack of precision in placing the desorption spot. By simple geometrical reasoning a 0.3 mm error in placing the middle spot moves the center of the profile by 10 mm, or one half-width, off-axis in the observation plane. Another part of the difficulty, and the probable cause of the jagged appearance of the horizontal profiles, was the nonuniform laser intensity within the desorption spot. Shot-to-shot variation of laser intensity also contributed to some extent, although the major irregularities were reproduced when two horizontal profiles were measured in succession. As illustrated in Fig. 6, small intensity variations cause large differences in the amount of perylene vaporized. Microscopic examination of the desorption spots confirmed uneven removal of the perylene film.

Some other sequences from which an estimate of the horizontal FWHM could be obtained yielded values of 16 mm for the middle, 10 and 13 mm for the outer spot. Profiles from the inner spot were too broad to be measured. The average widths observed are close to the widths of the straight-line projections of the desorption spots onto the observation plane, using tangents drawn from the edge of the jet orifice. These tangents may be viewed as approximate streamlines. For the middle spot the projection is 17 mm wide (obs. 16 and 22 mm), for the outer spot it is 11 mm wide (obs. 10 and 13 mm). It would obviously be interesting to measure the profile for a spot smaller than the jet orifice but we have not done this.

Time profiles measured in the wings of the horizontal distribution showed that the concentration maximum appeared at a given value of x somewhat later than at $y=0$. The additional delay was about as expected from the increased distance. This effect leads to a "lifting of the wings" of the horizontal profile since the maximum moves downward, in the $(-x)$ direction, with time. Although not clearly visible in Fig. 7, lifted wings were observed in some sequences. It thus appears that portions of desorbed material leaving the source at the same time travel in a plane and thus arrive at the same vertical position.

2.3. *Effect of Sample Position*

Results presented so far were obtained with a fixed distance between sample surface and jet axis, $x_s=-0.5$ mm. This distance turns out to be critical for the vertical position of the concentration maximum. Figure 9 shows a sequence of vertical profiles for varying sample position x_s. They represent the early portion of a desorption signal. It can be made to arrive with its peak above, at, or below the jet axis depending on the value chosen for $|x_s|$. For large values the signal is not only low on the x axis but also smaller, indicating less entrainment of desorbed perylene into the jet.

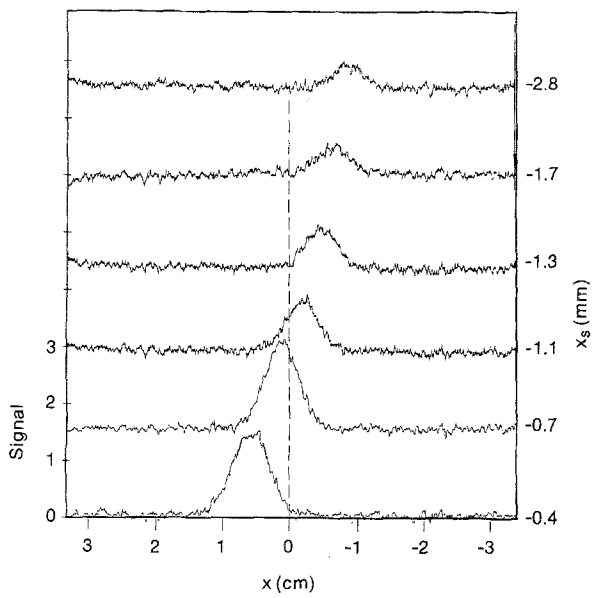

Fig. 9. Effect of sample distance from jet axis on the vertical profile (Delay: 38.5 μs, 3 mm spot)

Similar shifts of the vertical profile were observed at delay times longer than the ones shown in Fig. 9.

2.4. *Expansion into a Slot*

When the silica rod is moved close to the jet orifice, the gas first expands into a slot formed by the sample and rod surfaces. We investigated the effect of this constraint on the concentration profiles, hoping the rod would prove useful as an independent control element for shaping and aiming the concentration profile. At the settings used in experiments described so far the rod will be seen to have no influence on the profiles.

The effect of the second surface is most pronounced with the sample surface close to the orifice. Figure 10 shows a sequence of vertical profiles for varying rod distances with the sample at $x_s = -0.36$ mm. The profile begins to change at $x_q = 2.8$ mm. For $x_q = 2.8$ and 2.2 mm the profile is increasingly compressed on the upper (silica rod) side, which reduces its FWHM to 5 mm. For $x_q = 1.5$ and 0.9 mm the entire profile is shifted away from the rod surface, while the FWHM stays constant. Finally at $x_q = 0.6$ mm, the closest approach, the shift reverses and the width of the profile increases again. A similar sequence with $x_s = -0.52$ mm showed qualitatively the same behavior, including narrowing and shift reversal, but the shifts were smaller Variations in total area under the curves of Fig. 10 are probably not significant and due to laser intensity variation.

The interference of the rod surface with the jet expansion also produces an effect in the time domain. Figure 11 shows a composite of vertical profiles recorded at different delays with $x_q = 3.4$ mm (no interference) and $x_q = 0.9$ mm (strong interference), other conditions being the same as for Fig. 10. The arrival time of the peak concentration is delayed by about 2.5 μs when the rod interferes with the expansion.

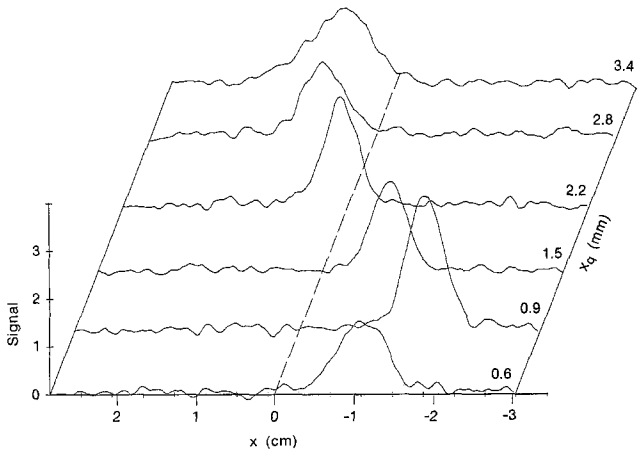

Fig. 10. Effect of squeezing the jet expansion with a second surface. $x_s = -0.4$ mm, $z_s = 0.7$ mm, delay 34 μs

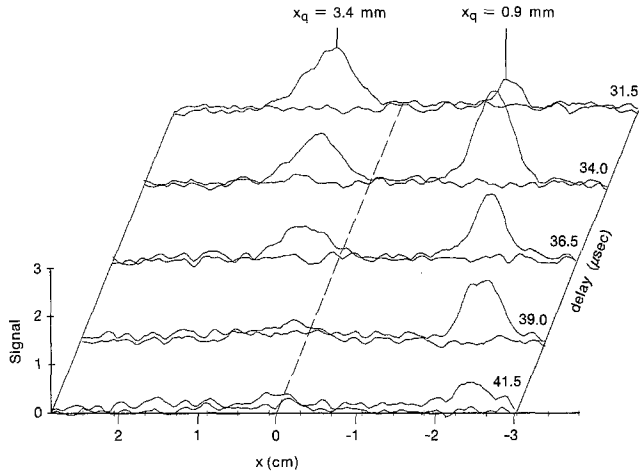

Fig. 11. Effect of the second surface on time evolution of the vertical concentration profile. Left time series is without, right series with second surface interference. $x_s = -0.4$ mm, $z_s = 0.7$ mm

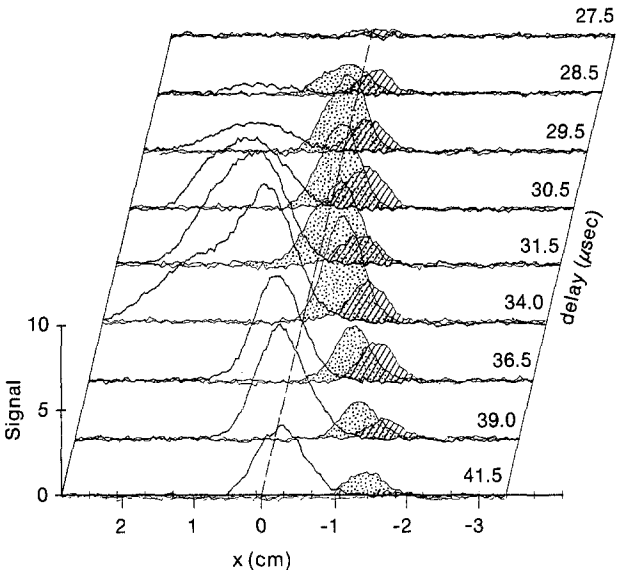

Fig. 12. Effect of source pressure on the vertical profile. This is a superposition of three time series, with source pressures of (from left to right) 1.0, 5.8, and 11.2 atm of He. $x_s = -0.5$ mm, $z_s = 0.7$ mm

2.5. *Variation of Source Pressure*

Reservoir pressure of the jet expansion is another parameter which strongly affects the position of the concentration profile. All results presented so far were obtained with He at 1 atm. Figure 12 shows what happens when the source pressure is increased to 5.8 and 11.2 atm. This figure is a composite of three separate time series of vertical profiles obtained at different source pressures, superimposed to facilitate comparison. The desorption pulse energy was at the high end of the range (55 to 60 μJ), therefore the 1 atm trace exhibits the typical overshoots encountered in

Sect. 2.1. Note that the time scale is expanded from 27.5 to 31.5 μs delay time in order to give a more detailed picture of the concentration pulse onset than do Figs. 2 to 5.

Four effects of the increase in source pressure are evident: The concentration maximum at a given delay shifts in the $(-x)$ direction, the highest concentration arrives somewhat earlier, the total amount of material passing the line of observation is reduced, and overshoots are suppressed. Apart from the overshoot effect which is prominent at 1 atm and barely noticeable at 5.8 atm, the FWHM of the profiles remains essentially the same as in experiments at lower desorption pulse energy and 1 atm of source pressure.

2.6. *Argon as Source Gas*

Some experiments in Ar were carried out to see whether the narrow, vertical profiles observed in He were related to the large perylene/He molecular mass ratio (252 : 4). The results are shown in Fig. 13 which is a superposition of two time series of vertical profiles recorded at Ar source pressures of 1.0 and 3.2 atm. These observations were made at intermediate desorption pulse energies of 45 to 50 μJ. Several differences with the He profiles are evident: The profiles in Ar are much broader and asymmetrical, especially at the lower pressure. The first signal and peak concentration appear somewhat earlier at the lower pressure. As in He an overshoot component is present at 1 atm source pressure which appears high on the x axis at intermediate delays. Observed time delays for the concentration maximum are 86.5 μs at 1 atm and 91.5 μs at 3.2 atm. When estimating the delay from the final expansion velocity of a room temperature Ar source one gets 100 μs. The discrepancy may be due to heating of the Ar reservoir by the magnet coils of the pulsed valve, an effect which would be less noticeable with He due to its higher thermal conductivity. An Ar source temperature of 90 °C gives a velocity which agrees with the observations.

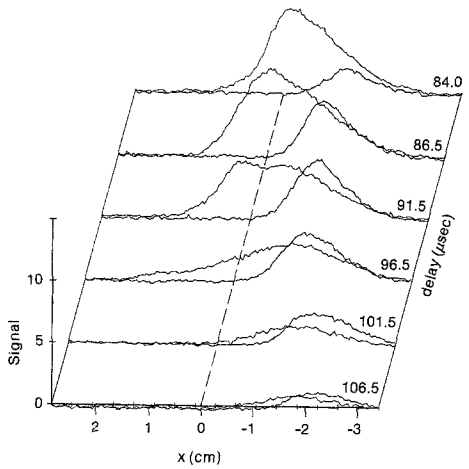

Fig. 13. Time evolution of the vertical profile with Ar as source gas. This is a superposition of two series, with source pressures of (from left to right) 1.0 and 3.2 atm of Ar. $x_s = -0.5$ mm, $z_s = 1.7$ mm

Two time series, one with He and another with Ar at 1 atm, were recorded using identical settings and approximately equal desorption pulse energy. The total signal areas summed over time were 1500 units for Ar and 1200 units for He. Since the difference is within the range attributable to small changes in laser intensity, the total amount of material entrained with Ar and He under identical conditions is probably the same. The maximum on-axis signal for He was, however, almost twice as large as for Ar due to the smaller width of the concentration profile.

3. Discussion

3.1. *Concentration Profiles*

Quantitative modeling of the observed concentration profiles would be a formidable task, involving the flow dynamics of the perturbed jet expansion interacting with with that of the laser-induced desorption process. We have not attempted to do this. It is likely that shock fronts in the expansion caused by the obstructions, as well as shock waves produced by the laser pulse, play a role. An indication of the former is present in the results described in Sect. 2.4 where expansion into a slot caused a zig-zag motion of the concentration profile as the slot was made narrower.

Jet-like pulses of desorbed material are evident in many of the vertical profiles observed at high desorption laser intensity and low source pressure, such as in Figs. 4, 5, 12, and 13. They show up as an asymmetrical broadening on the $(+x)$ side when the profile is compared with that obtained at low intensity. We call them jet-like because they appear only at delay times which, as will be argued below, correspond to the arrival of material injected vertically. It is possible that this phenomenon is caused by shock waves or other perturbations of the jet density. We prefer an explanation which assumes that the density in the jet (which is in its steady state) stays constant. An extra, high-velocity component of vaporized sample is generated which penetrates farther into the expanding gas. This extra component has an angular distribution which strongly peaks in the vertical direction and thus is not seen in the later portions of the signal. Similar effects in laser-induced desorption have been seen by other investigators [14]. These pulses are strongly suppressed, or their range shortened, at higher source pressures.

As illustrated by Fig. 7 the two-dimensional concentration profiles produced by our experimental arrangement are ridge-shaped, with the ridgeline running parallel to the sample plane. The horizontal width

of the profile appears to correspond with the projection of the desorption spot onto the observation plane. Vertical sections have a Gaussian shape for He, are very narrow compared with the FWHM of the jet density, and are remarkably independent of delay time, source pressure, desorption geometry, and horizontal position. For Ar vertical profiles are broader and asymmetrical. If the vertical widths were determined by simple diffusion we would expect them to be larger in He. Since the opposite is observed, it seems more likely that a gas-dynamic separation effect is responsible which increases with molecular mass ratio and thus is more effective in He.

It is known that Ar will cause clustering under the conditions of our experiment. Our detection technique does not discriminate between free perylene molecules and those clustered with Ar. Since clustering will only begin when the perylene is accommodated in the expansion, we believe that it will not significantly affect the concentration profiles. Observations by photoionization mass spectrometry showed that in the He expansion perylene is mostly monomeric.

A common feature in all our time profiles is the downward motion of the concentration maximum with delay time. One may try to explain this by attributing the length of the concentration pulse to the duration of sample vapor emission, and the downward motion to a shorter penetration depth of the vapor as the sample surface cools down following the desorption pulse. The first part of this explanation doesn't fit the results because the concentration pulse is longer in Ar (ca. 20 μs FWHM) than in He (ca. 13 μs FWHM). The second part is contradicted by the results presented in Fig. 6 which show that vertical position is independent of sample temperature as long as the high-intensity overshoot effects don't interfere. We speculate that the downward motion reflects portions of desorbed material injected into the expansion with different velocity components. Portions with a large, positive z component arrive first and highest on the x axis since they were injected in the direction of lowest density. Desorption further away from the nozzle should then cause the signal to appear at higher x values, as observed. Portions with a small z component, injected vertically, constitute the main fraction (thus we compared predicted flight times with the delay time of the concentration maximum). This is consistent with the appearance of the jet-like overshoot features in high intensity runs at delay times corresponding to peak concentration in low-intensity runs. Portions with negative z components, injected toward the high density side of the jet, and portions injected with low initial velocity, make up the late parts of the signal appearing low on the x axis.

Similar arguments based on density effects would also qualitatively explain why vertical profiles at equal delay times are shifted down on the x axis when the source pressure is increased (Fig. 12). A shorter penetration depth at higher density will increase the amount of vaporized material recondensing on the sample surface, which may explain the decrease of the total signal at higher source pressure. Fluorescence probing in the sample region with higher spatial and temporal resolution would be necessary to get a better understanding of the entrainment and focusing processes.

3.2. *Applications*

Narrow concentration profiles, especially in He, combined with the ability of aiming them, are a considerable advantage for applications of the entrainment technique. The fraction of entrained material which is extracted through a skimmer centered on the jet axis can be made much larger than the fraction of expansion gas passing through the skimmer. To optimize this fraction the profile maximum should be approximately on axis at the delay time corresponding to peak concentration. The two preferred control parameters for achieving this are sample height and source pressure. A second control surface above the jet orifice can also be used. While this has some advantage in producing still narrower concentration profiles, the disadvantages may be more significant: Interference with the expansion causes reduced final velocity and higher final temperature, and constant transparency of the second surface for the desorption beam may be hard to maintain due to coating by desorbed material.

We will estimate the fraction of entrained material which can be extracted as a packet of convenient size for laser detection by using the time series of Fig. 3, which is nearly optimal, and the horizontal profile of Fig. 8. Because of the elongated shape of the two-dimensional profile it is advantageous to use a slit skimmer; we are employing one with a 4×1 [mm] cross-section. This slit will pass about 8×10^{-4} times the total gas flow at the 57 mm sampling distance used in this work [13]. The fraction of entrained perylene passing through the skimmer is estimated by approximating the perylene flux, $F(t)$, as

$$F(t)dx\,dy = pv(x,t)h(y)dx\,dy \tag{1}$$

where $v(x,t)$ is given by the profiles in Fig. 3, $h(y)$ by the profile in Fig. 8, and p is a proportionality constant. If the skimmer is ideal the fraction, f, sampled between the delay times t_1 and t_2 is

$$f = \frac{\int_{\frac{-w}{2}}^{\frac{w}{2}} h(y)dy \int_{t_1}^{t_2} dt \int_{\frac{-h}{2}}^{\frac{h}{2}} v(x,t)dx}{\int_{-\infty}^{\infty} h(y)dy \int_{0}^{\infty} dt \int_{-\infty}^{\infty} v(x,t)dx}, \tag{2}$$

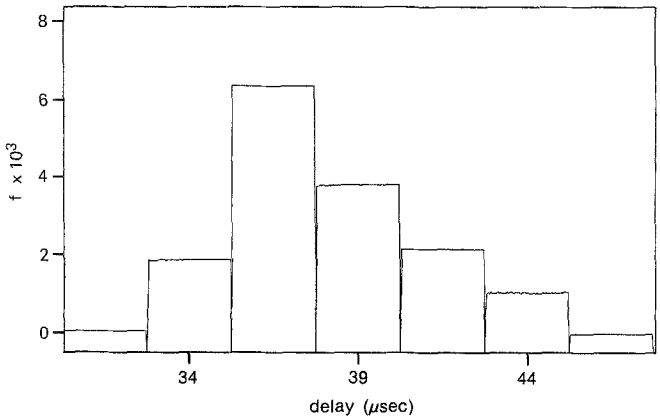

Fig. 14. Fractions of entrained material vs. time, for 2.5 μs time intervals, passing through a 1×4 [mm] skimmer at 57 mm sampling distance. The calculation was based on the vertical profiles of Fig. 3 and the horizontal profile of Fig. 8, using (2)

where w and h are the width and height of the skimmer. Figure 14 shows a histogram of f with the time interval $t_2 - t_1 = 2.5$ μs moved across the pulse in 2.5 μs steps. Its total area corresponds to 1.5% of the entrained material. The 5 μs packet from 35.3 to 40.3 μs delay time is 9 mm long in the z direction at the final He expansion velocity; a laser beam of that width, traveling in the y direction, would interact with 1.0% of the entrained material. Of course, this fraction will vary with skimmer size, nozzle-to-skimmer distance, and with the volume chosen for the interaction region.

The horizontal fraction captured by the skimmer can be increased by moving the desorption spot further from the nozzle and by decreasing its diameter, thereby narrowing the horizontal concentration profile. Since distance from the nozzle will affect the degree of cooling, this parameter must be optimized depending on the application. Precise alignment of the desorption spot along the jet axis is important.

While we have not addressed the issue of final temperature in this work, some preliminary experiments with tryptophan films showed that the entrained material is effectively cooled, contrary to observations made by Tembreull and Lubman with a different entrainment geometry [15]. With our experimental arrangement linewidths of 1.2 cm^{-1} in the two-photon ionization spectrum were observed. This is about two times narrower than the widths reported by Rizzo et al. for a pulsed nozzle with a long, heated throat [16]. It was possible to scan a 150 cm^{-1} portion of the spectrum using a single desorption spot on a thick, polycrystalline film and about 2000 desorption pulses.

4. Conclusions

We have investigated how perylene, laser-desorbed from a flat surface in front of a pulsed nozzle, is entrained in the jet expansion and distributed in space and time far from the nozzle. With He as the expansion gas we found the perylene focused in a small part of the jet cross-sectional area, within a ridge-like concentration profile that is parallel to the sample surface and sweeps in the direction perpendicular to it with time. Our results show how the experimental parameters influence the shape and time trajectory of this profile and thus how the overlap of the concentration pulse with a skimmer or other probe can be optimized. We estimated that with our particular arrangement, which is not optimized, about 1.0% of the entrained vapor can be extracted through a skimmer in the form of a $1 \times 4 \times 9$ mm^3 packet. We therefore conclude that the entrainment technique should have useful sensitivity for identifying molecules adsorbed on surfaces by resonant multiphoton ionization or fluorescence spectroscopy, in cases where the adsorbate lends itself to these methods of detection.

References

1. D.H. Levy: Science **214** (4518), 263 (1981)
2. M.A. Posthumus, P.G. Kistemaker, H.L.Z. Meuzelaar, M.C. Ten Noever de Brauw: Anal. Chem. **50**, 985 (1978). The following, more recent publications contain partial bibliographies: F. Engelke, J.H. Hahn, W. Henke, R.N. Zare: Anal. Chem. **59**, 909 (1987); C.L. Wilkins, D.A. Weil, C.L. Yang, C.F. Ijames: Anal. Chem. **57**, 520 (1985)
3. R.B. Hall: J. Phys. Chem. **91**, 1007 (1987)
   M.G. Sherman, J.R. Kingsley, J.C. Hemminger, R.T. McIver, Jr.: Anal. Chim. Acta **178**, 79 (1985)
4. H. v. Weyssenhoff, H.L. Selzle, E.W. Schlag: Z. Naturforsch. **40a**, 674 (1985);
   J. Grotemeyer, U. Boesl, K. Walter, E.W. Schlag: J. Am. Chem. Soc. **108**, 4233 (1986); Org. Mass Spectr. **21**, 645 (1986)
5. R. Tembreull, D. Lubmann: Anal. Chem. **58**, 1299 (1986); **59**, 1003 (1987); **59**, 1082 (1987)
6. S.L. Shapiro, R.C. Hyer, A.J. Campillo: Phys. Rev. Lett. **33**, 513 (1974)
   C. Bouzou, C. Jouvet, J.B. Leblond, Ph. Millie, A. Tramer, M. Sulkes: Chem. Phys. Lett. **97**, 161 (1983)
7. Y. Kamura, K. Seki, H. Inokuchi: Chem. Phys. Lett. **30**, 35 (1975)
8. Model BV-100, Newport Corp., Fountain Valley, Ca. 92728
9. Hyperex-400 Series, Lumonics Inc., Kanata, Ont., Canada K2X 1Y3
10. KYNAR Piezo Film, Pennwalt Corp., King of Prussia, Pa. 19406
11. Model DCR-2, Quanta Ray Div. of Spectra Physics, Mt. View, Ca. 94043
12. OMA-1 with Mod. 1420 Detector, EG&G Princeton Applied Research, Princeton, NJ 08543
13. H. Ashkenas, F.S. Sherman: Proc. 4th Int. Symp. Rarefield Gas Dynamics, Vol. 2, Suppl. 3, 84 (1964)
14. K. Domen, T.J. Chuang: Phys. Rev. Lett. **59**, 1484 (1987)
15. R. Tembreull, D. Lubman: Appl. Spectr. **41**, 431 (1987)
16. T.R. Rizzo, Y.D. Park, L.A. Peteanu, D.H. Levy: J. Chem. Phys. **84**, 2534 (1986)